Supporting Information

Greatly enhanced anticorrosion of Al–AlN_xO_y nanocermet films with self-passivated Al nanoparticles for enduring solar-thermal energy harvesting

Chengbing Wang,*[a] Zhengtong Li,[a] Weike Wang,[a] Rongbin Xia[b] and Xiaoming Ling*[c]

[a]*School of Materials Science and Engineering, Shaanxi Key Laboratory of Green Preparation and Functionalization for Inorganic Materials, Shaanxi University of Science and Technology, Xi'an, Shaanxi 710021, China*

[b]*Changzhou Dacheng Green Coating Technology Co. LTD, Changzhou, Jiangsu 213001, China*

[c]*National Engineering Research Center for Technology & Equipment of Green Coating, Lanzhou Jiaotong University, Lanzhou 730070, China*

Section 1. The composition and the structure of the reference samples.

Copper and aluminum are traditionally used as substrates in solar collectors because of their high thermal conductivity and high IR reflectance. So we selected two typical commercial cermet SSACs named 2–Al coated on Al substrate and 3–Cu coated on Cu substrate, respectively, for comparing.

Sample 2–Al was produced by ALMECO-TINOX GROUP, which is a 100-nm-thick reactive evaporated titanium oxy-nitride layer on aluminum substrate, the antireflective layer is 100 nm thick SiO_2 (Fig. S1a). [1]

Sample 3–Cu is commercial PVD coatings (Sunselect, Alanod) with excellent spectral selectivity, which is a cermet material consisting of metallic nanoparticles embedded in a ceramic matrix. Sunselect is a bilayer coating consisting of a 30 nm thick SnO_2 anti-reflective layer on the top of the 90 nm-thick CrN_xO_y layer, the Sunselect coating was deposited directly on the Cu substrate (Fig. S1b). [2]

The layer structure of Al–AlN_xO_y SSACs is shown in Fig. S1c. The coating is composed of four ordinal layers: Al_2O_3 barrier layer, Al–AlN_xO_y with a high metal volume fraction (HMVF), Al–AlN_xO_y with a low metal volume fraction (LMVF) and an AlN_xO_y anti-reflection (AR) layer.

In this paper, for sample 2-Al and sample 3-Cu, it is not the main object of our analysis. It is mainly used to compare the optical properties, thermal stability and corrosion resistance of the Al-AlN_xO_y SSACs, demonstrating the excellent optical and corrosion resistance of the Al-AlN_xO_y SSACs.

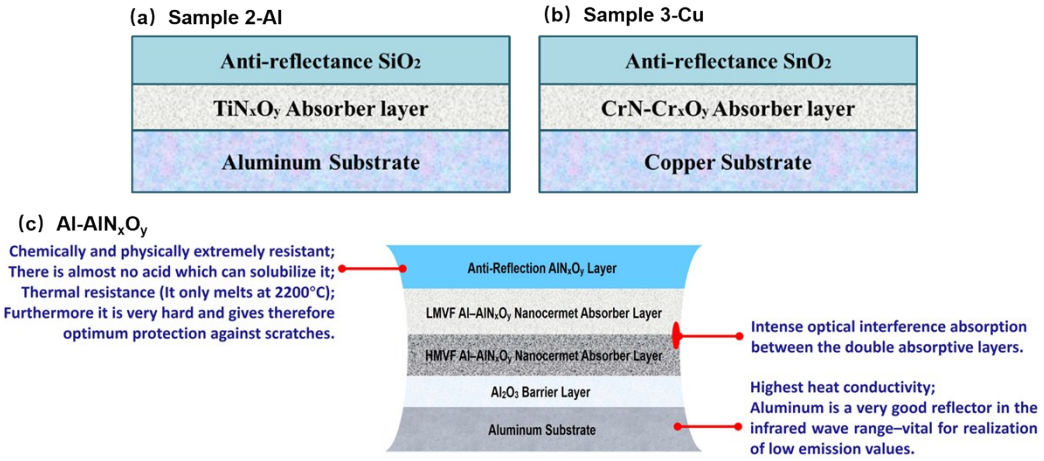

Fig. S1. The structural characteristics of (a) Sample 2-Al, (b) Sample 3-Cu and (c) Al-AlN_xO_y SSACs.

Section 2. Thermal stability and phase structure of Al–AlN_xO_y SSACs.

Thermal stability of Al–AlN_xO_y SSACs in air (300 °C and 350 °C) was investigated in an accelerated test performed in a circulating air furnace. The long-term vacuum thermal stability of the samples was investigated in a vacuum annealing furnace, when chamber vacuum pressure was better than 4×10^{-4} Pa, the samples were rapidly heated up to 400 °C and then cooled down to room temperature after an interval of ~50 h (one cycle in our case), followed by the repeating heat treatment cycle. The performance criterion (PC) is a useful criterion that describes the influence of changes of the solar absorbance ($\Delta\alpha_s$) and thermal emissivity ($\Delta\varepsilon$) with respect to the solar fraction: $PC = -\Delta\alpha_s+0.5\Delta\varepsilon \leq 0.05$. [3]

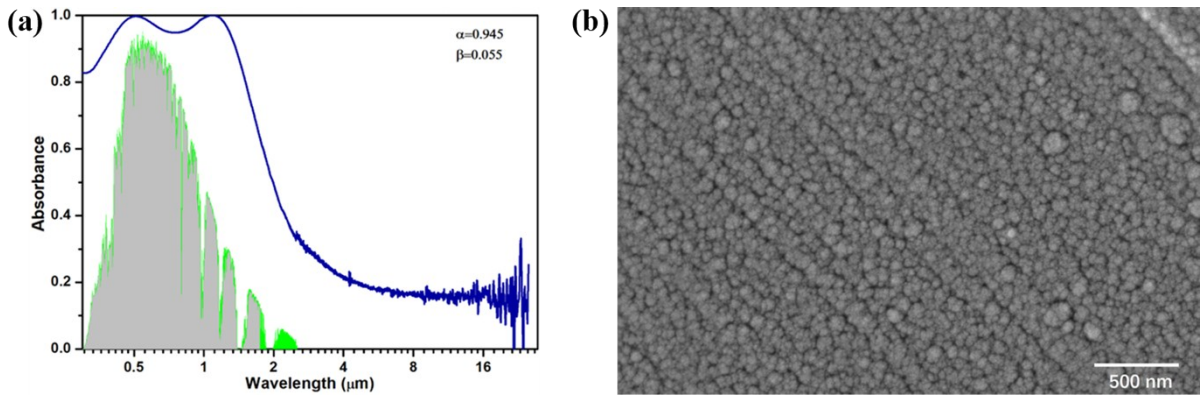

Fig. S2. Spectral absorbance curve (a) and the surface morphology of the Al–AlN_xO_y SSACs (b).

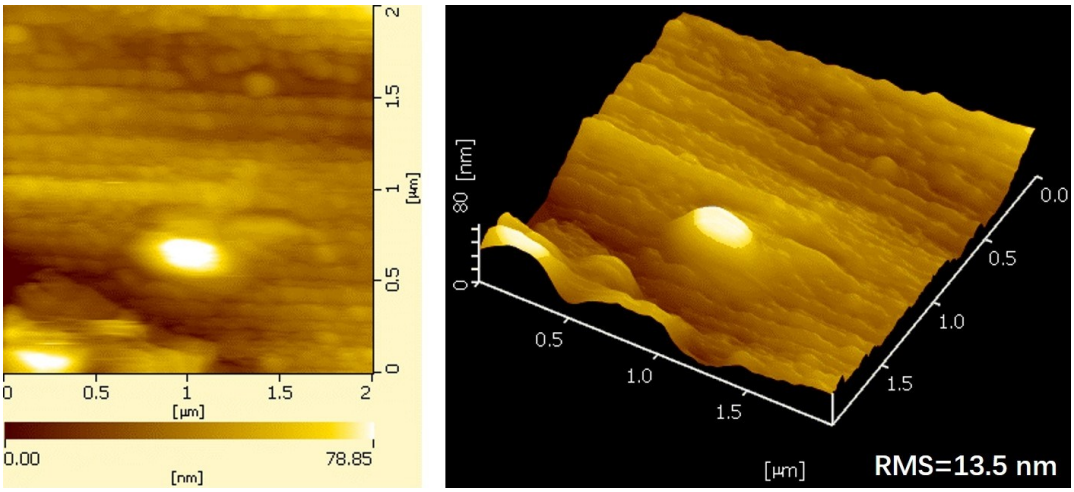

Fig. S3. 2D and 3D AFM images of the Al–AlN_xO_y SSACs on aluminum substrate.

It is clear that the Al–AlN_xO_y SSACs was stable up to a temperature of 300 °C for 300 h (Table 1). The PC values is as low as 0.009 after annealing at 300 °C for 300 h, show an excellent thermal stability. At 350 °C (200 h), the absorptance values lightly decreased from 0.950 to 0.903, and there was no change in the emissivity as listed in Table 1, the PC value (0.022) was slightly low the qualifying criterion (PC<0.05). It indicates that Al–AlN_xO_y SSACs is available for solar-thermal collector. The absorber surface is considered qualified since the PC value of 300 °C for 75h (-0.031) is greater than the PC value of 250 °C for 200h (-0.022), as per the recommendations of IEA SHC.[4] These results show that the Al–AlN_xO_y SSACs has qualified the accelerated aging test and the minimum service life time of the absorber is estimated to be 25 years.

The shape of Raman spectra of the coating did not show notable change even after heating to a temperature of 350 °C in air (Fig. S4a, b). These results indicate no significant changes in the structure of the Al–AlN_xO_y SSACs even after heat treatment in air at 350 °C for 75 h.

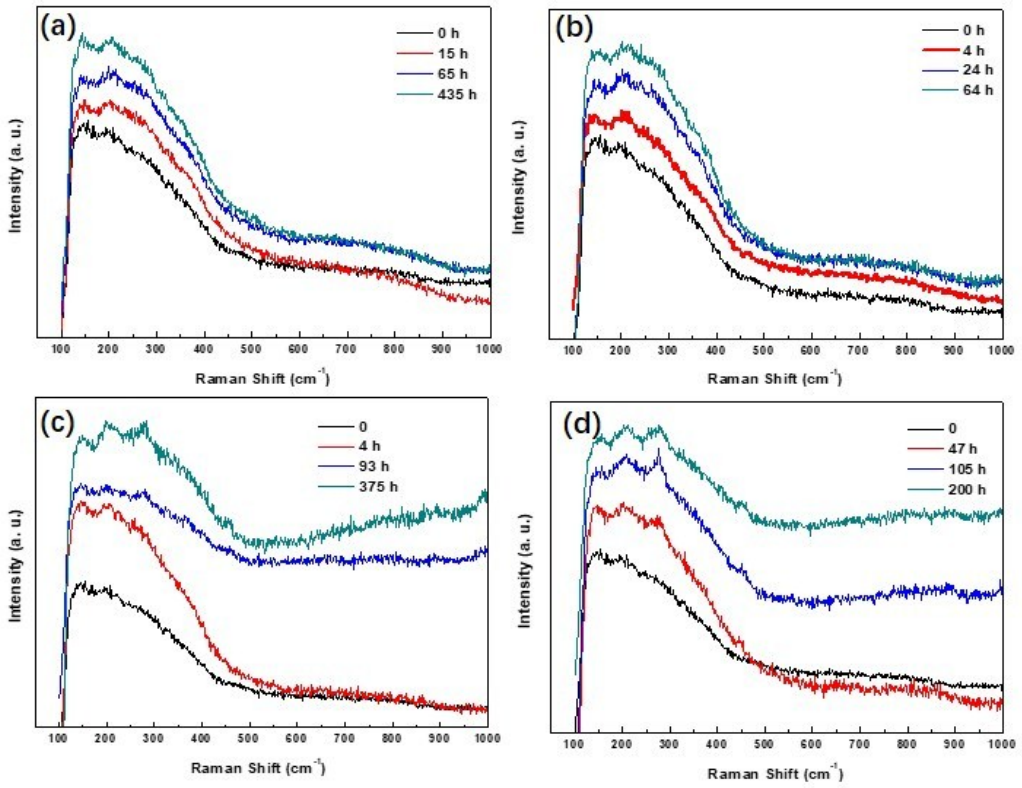

Fig. S4. Comparative micro-Raman spectra of Al–AlN_xO_y SSACs and heat treated (a) 300 °C in air, (b) 350 °C in air, (c) 400 °C in vacuum, and (d) 450 °C in vacuum.

The Al–AlN_xO_y SSACs was also subjected to heat-treatment for durations at 400 °C and 450 °C in vacuum (5.0×10^{-4} Pa). The absorptance and emissivity values of the absorber coating are summarized in Table 1.

As can be seen from Table 1, the coating retains its optical properties for temperature less than 450 °C. At 450 °C, the absorptance decreased drastically (-0.246) and the emissivity increased (+0.04). As we know in the Al–AlN_xO_y SSACs, metal aluminum nanoparticles (NPs) embedded in dielectric AlN_xO_y matrix, we also notice that aluminum has a lower melting point (660 °C), hence diffusion and mobility of Al NPs are very strong, which lead to merge of Al NPs each other, so the structure of the coating was damage, thus the optical performance was degrade sharply at 450 °C. Therefore, thermal stability tests were conducted for longer heating durations at 400 °C. Vacuum annealing up to 400 °C for 375 h did not significant affect the absorptance (-0.004) and the emissivity values (-0.04) of the Al–AlN_xO_y

SSACs. No structural changes were observed as a result of prolonged heating, as confirmed using Raman studies (Fig. S4c, d) and XRD (Fig. S5). This demonstrates that the Al–AlN_xO_y SSACs can be used in vacuum where in the temperature is less than 400 °C (for example, receiver tubes).

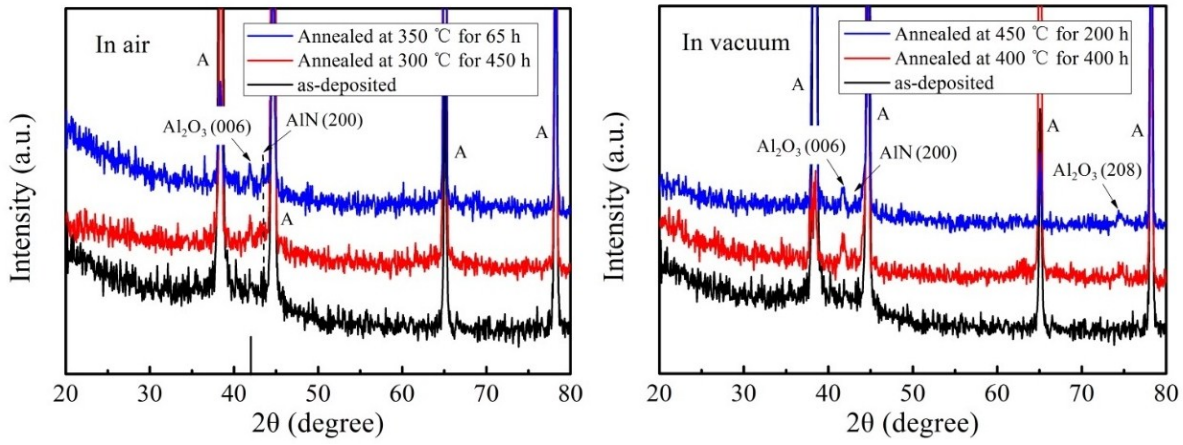

Fig. S5. XRD spectra of Al–AlN_xO_y SSACs after annealed in air and in vacuum for different conditions.

Fig. S5 depicts the XRD spectra of Al–AlN_xO_y SSACs after annealed in air and in vacuum for different conditions. During annealing in air, aluminum elements were partially oxidized, yielding to crystalline Al_2O_3 peak located at 2θ=42.0º.[5–7] The weak peaks at 43.4º can be assigned to AlN (200).[5–7] As annealing temperature rose, the peaks Al_2O_3 and AlN were winded, indicating oxidation has been aggravated. When annealed in vacuum, the crystalline Al_2O_3 peaks (2θ=41.7º) also could be identified, being aluminum and oxygen element from antireflective layer. In addition, a weak peak at 74.5º corresponded to (208) plane of Al_2O_3.[5–7]

The change in surface morphology of Al–AlN_xO_y SSACs after annealing in air and vacuum is different. With the increase of annealing temperature in air, the surface became rougher. Abnormal grain growth (Fig. S6a–c) appeared in the surface of the coatings. With increasing annealing time, particle size continuously increases in an indiscernible manner, and no microscopic holes and cracks were observed. Despite the growth in particle size, the particles

remained uniform and compact after annealing at 350 °C for 64 h in air (Fig. S6c). The changes in surface morphology after annealing may also cause a change in the optical performance of the coatings. However, as the coating annealing in vacuum, a slight grain agglomeration was observed (Fig. S6d–f), abundant cracks were generated when annealing for 200 h in vacuum at 450 °C (Fig. S6f), the grain size almost keep the same as-deposited coating. So, it can be deduced that the volume expansion would produce local stress and therefore result in formation of micro-cracks, wider grain boundaries.

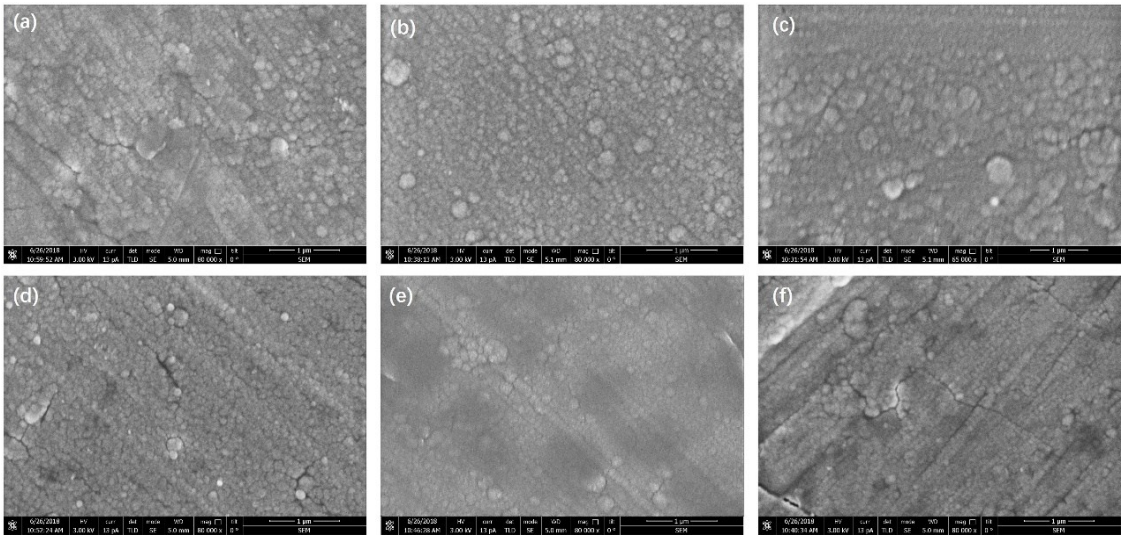

Fig. S6. Effect of annealing on surface morphologies of Al–AlN_xO_y SSACs. (a) 300 °C for 35 h in air, (b) 350 °C for 14 h in air, (c) 350 °C for 64 h in air, (d) 400 °C for 375 h in vacuum, (e) 450 °C for 47 h in vacuum, (f) 450 °C for 200 h in vacuum.

Section 3. Salt spray corrosion of Al–AlN_xO_y SSACs.

The corrosion stability of the samples was examined by exposing the samples to a neutral salt spray (NSS) test according to the ASTM B117 standard (5% NaCl, pH 6.5 to 7.2, 35 °C).[2] After each corrosion experiment, the samples were first ultrasonically washed with deionized water for 10 min and then rinsed with deionized water twice to remove surface residues. We selected two typical commercial used solar absorber coatings, named 2–Al and 3–Cu, respectively, for comparing. All the coatings were prepared by magnetron sputtering. Sample 2–Al is cermet absorber coating on aluminum substrate, and sample 3–Cu is cermet

absorber coating on copper substrate.

Table S1. Optical properties of Al–AlN_xO_y SSACs corroded in different time.

Time (h)	**α**	**ε**	**$\Delta\alpha_s$**	**Δε**	**PC**	**α/ε**
0	0.945	0.055	0	0	0	17.18
10	0.945	0.048	0	-0.007	-0.0035	19.69
15	0.956	0.042	0.011	-0.013	-0.0175	22.76
20	0.953	0.045	0.008	-0.010	-0.013	21.18
40	0.950	0.051	0.005	-0.004	-0.007	18.63
80	0.942	0.058	-0.003	0.003	0.0015	16.24
100	0.941	0.065	-0.004	0.010	0.009	14.48
387	0.940	0.071	-0.005	0.016	0.013	13.24
630	0.939	0.075	-0.006	0.020	0.016	12.52
782	0.934	0.081	-0.011	0.026	0.024	11.53
948	0.930	0.087	-0.015	0.032	0.031	10.69
1130	0.928	0.090	-0.017	0.035	0.0345	10.31
1290	0.924	0.095	-0.021	0.040	0.041	9.73
1404	0.921	0.098	-0.024	0.043	0.0455	9.40
2000	0.920	0.116	-0.025	0.061	0.0555	7.93

Table S2. Optical properties of commercial sample 2–Al corroded in different time.

Time (h)	α	ε	**$\Delta\alpha_s$**	**Δε**	**PC**	**α/ε**
0	0.965	0.050	0	0	0	19.3
23	0.930	0.050	-0.035	0	0.035	18.6
30	0.934	0.051	-0.031	0.001	0.0315	18.31
46.5	0.927	0.054	-0.038	0.004	0.040	17.17
53	0.928	0.054	-0.037	0.004	0.039	17.19
70	0.924	0.055	-0.041	0.005	0.0435	16.8
94	0.925	0.056	-0.040	0.006	0.043	16.52
100	0.924	0.056	-0.041	0.006	0.044	16.5
118	0.911	0.060	-0.054	0.010	0.059	15.18
146	0.906	0.082	-0.059	0.032	0.075	11.05
169	0.909	0.083	-0.056	0.033	0.0725	10.95
191	0.906	0.089	-0.059	0.039	0.0785	10.18
210	0.904	0.097	-0.061	0.047	0.0845	9.32
282	0.901	0.145	-0.064	0.095	0.1115	6.21
630	0.894	0.297	-0.071	0.247	0.1945	3.01

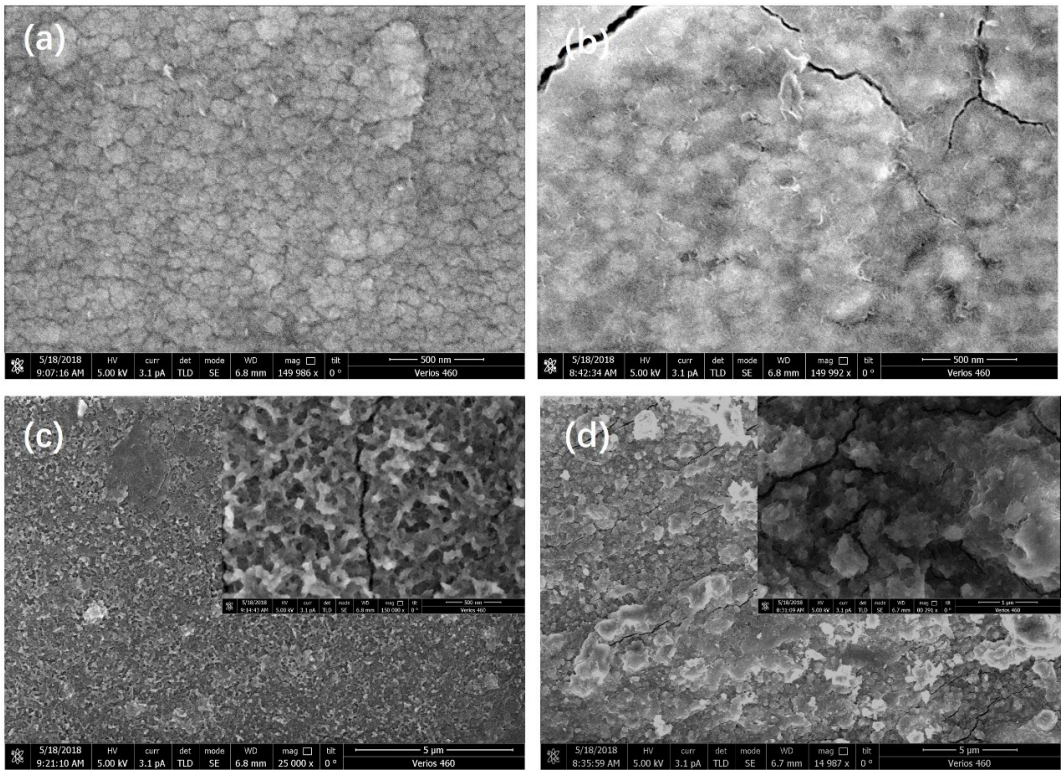

Fig. S7. Surface morphology of Al–AlN_xO_y SSACs as-deposited and corroded in 5.0% NaCl salt spray corroded for (a)10 h, (b) 100 h, (c) 948 h, (d) 2000 h. The inset in (c) and (d) are high-magnification picture.

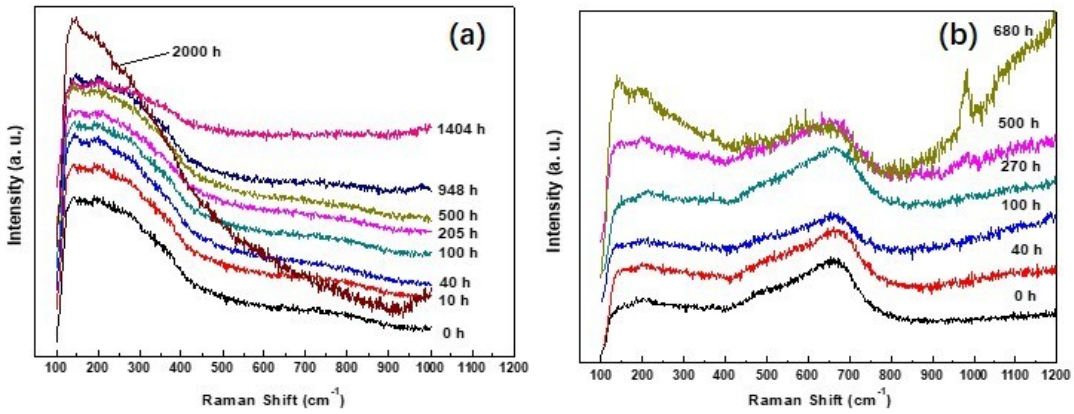

Fig. S8. Comparative micro-Raman spectra of (a) Al–AlN_xO_y SSACs and (b) sample 2–Al corroded by 5.0 wt % neutral salt spray.

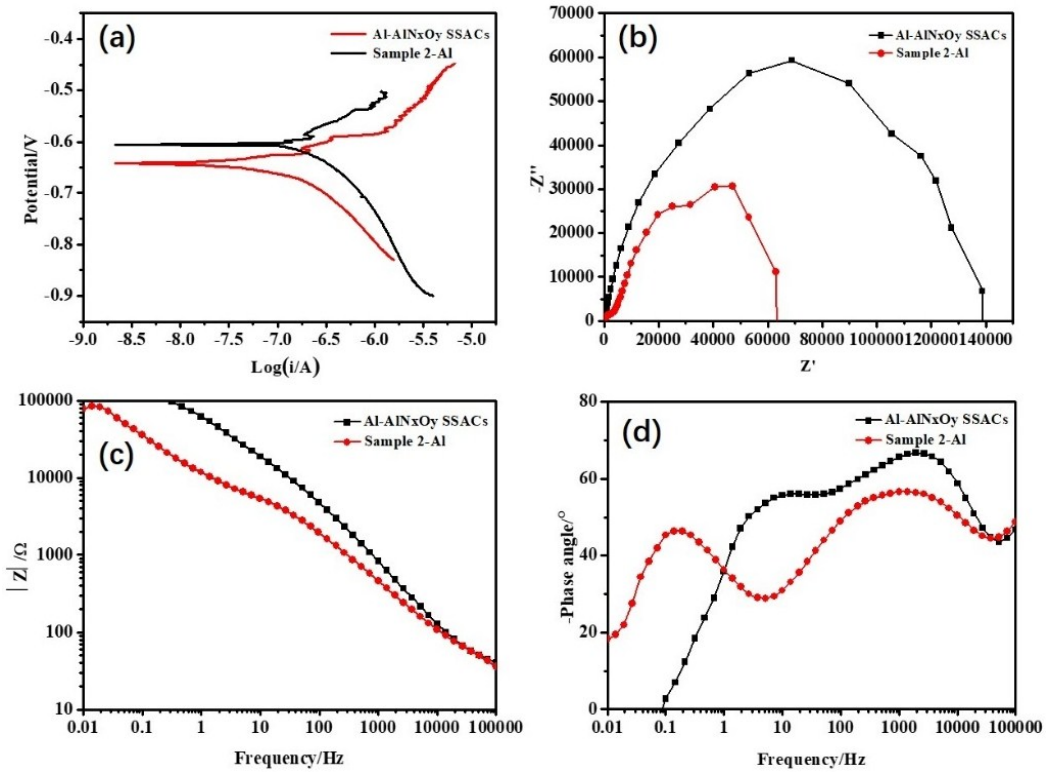

Fig. S9. Tafel curves (a), Nyquist plots (b), Bode plots (c) and (d) phase angle plot of Al–AlN_xO_y SSACs and sample 2–Al.

In order to evaluate the corrosion resistance of the Al–AlN_xO_y SSACs, the potentiodynamic polarization curve was measured after the neutral salt spray test (Fig. S9a). The corrosion electrode potential of Al–AlN_xO_y SSACs is -0.6 V, while the sample 2–Al is about -0.65 V. In addition, the corrosion current of Al–AlN_xO_y SSACs is smaller than that of the sample 2–Al. The results show that Al–AlN_xO_y SSACs have better corrosion resistance than sample 2–Al. Fig. S9b is a Nyquist plot. As the real part Z' of the impedance increases, the corrosion resistance of Al–AlN_xO_y SSACs is better than that of the sample 2–Al. The distance from any point on the semicircle to the origin represents the amplitude gain of the frequency at that point. The larger the value, the better the corrosion resistance of the coating. Obviously, the corrosion resistance of Al–AlN_xO_y SSACs is best. Fig. S9c is a plot of impedance versus frequency. As the frequency increases, the impedance of the experimental sample is larger than that of the sample 2–Al, which indicates that Al–AlN_xO_y SSACs has the best anti-corrosion performance. The higher the impedance, the greater the polarization resistance of

the coating. This indicates that the fewer defects in the sample, the better the corrosion resistance. Fig. S9d shows the change of phase angle with frequency. When the frequency is greater than 10000 Hz, the phase angle of Al–AlN_xO_y SSACs is larger than that of the sample 2–Al, indicating that the test sample has better corrosion resistance. A hesitation process occurs in the high frequency band, which is related to the coating and solution interface and reflects the dielectric properties of the coating itself. In the high frequency band, the larger the phase angle, the better the corrosion resistance.

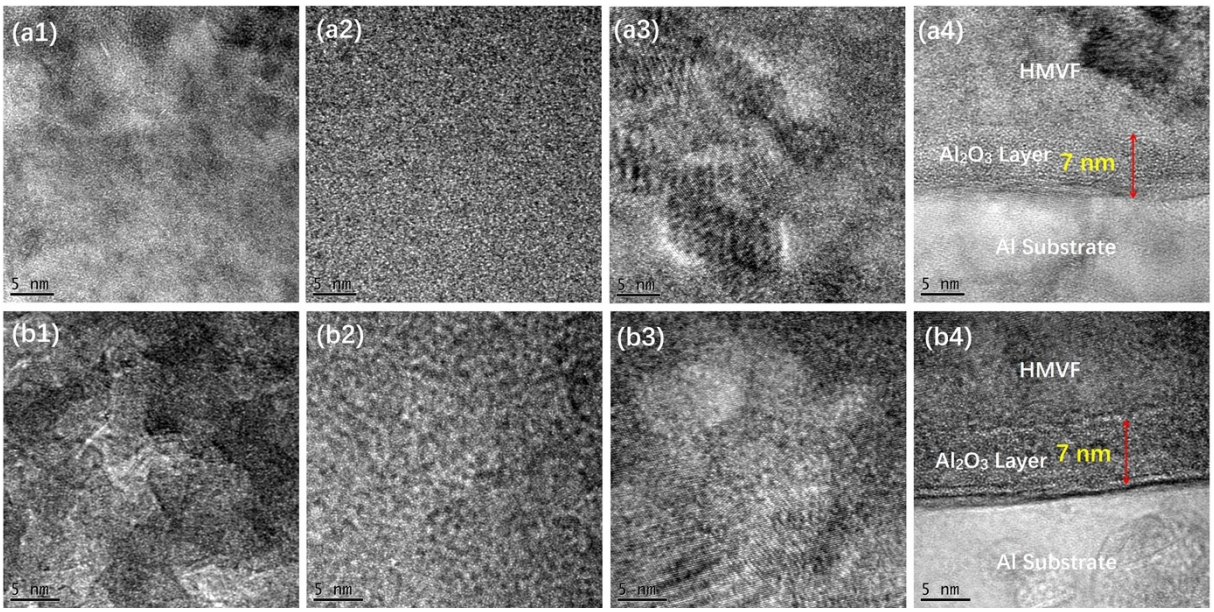

Fig. S10. Cross-sectional HRTEM images of (a1–a4) pristine Al–AlN_xO_y SSACs and (b1–b4) after annealing corrosion for 2000 h. (a1, b1) AR layer, (a2, b2) LMVF layer, (a3, b3) HMVF layer, and (a4, b4) the interface between Al bonding layer and Al substrate.

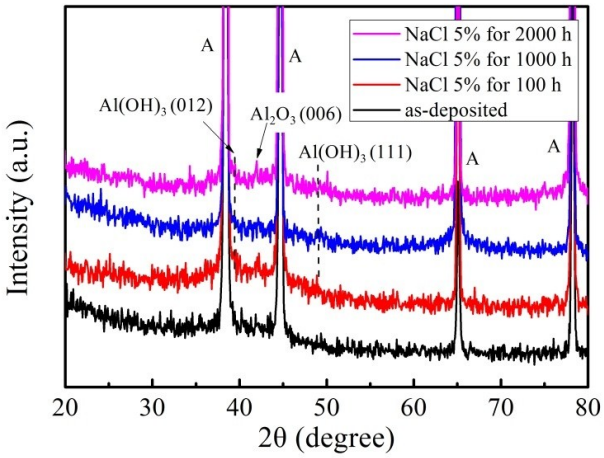

Fig. S11. The XRD spectra of Al–AlN_xO_y SSACs corroded by 5 % NaCl salt spray.

Fig. S11 shows the XRD spectra of Al–AlN_xO_y SSACs after corroded by 5 % NaCl salt spray. These peaks at 38.4º, 44.8º, 65.3º and 78.4º (marked by A) correspond to Al substrate. After corroding reaching 100 h, Al–AlN_xO_y SSACs present some new peaks at 39.5º, 41.7º and 49.01º, and which can be ascribed to $Al(OH)_3$ (012), Al_2O_3 (006), Al(OOH) (051).[5–7] And those diffraction peaks are widened as corroding time increased to 2000 h. This suggested that aluminum element yielded to variety of corrosion products, including alumina, aluminum oxide hydroxide and aluminum hydroxide, and the XRD results did not found aluminum chloride.

Table S3. The relative total energies of complex, surface and molecule, and the absorbtion energies of two models.

Model	**Complex**	**Surface**	**Molecule**	**E_{abs}**
Al (111)	-50.24	-32.83	-8.77	-8.63
Al (111)/Al_2O_3/OH	-199.05	-189.36	-8.74	-0.95

Section 4. Industrial air-to-air produce of Al–AlN_xO_y SSACs.

The self-developed industrial air-to-air magnetron sputtering line (ZDJ–WX–1250) was used to continuous produce Al–AlN_xO_y SSACs on Al strip at a line speed of up to 1 m/min (Fig. S12). Some important technical data are compiled in Table S4. The layer structure of Al–AlN_xO_y SSACs is shown in Fig. S1c. Aluminum is a kind of substrate material that is widely used in SSACs due to high spectra reflectivity, low thermal emissivity, high thermal conductivity and lower price relative to copper. Chemical components of aluminum strip (Al 1050) are shown in Table S5.

Fig. S12. Photo of the self-developed air-to-air produce line with a length of 90 m and a height of 2.5 m which was used to continuous fabricate large-scale Al–AlN_xO_y SSACs on Al strip. (a) panoramic photo, (b) overlooking photo, (c, d) panoramic photo from one side, (e) un-winding roller, and (f) re-winding roller.

Table S4. Important technical data of the ZDJ–WX–1250 production line.

Kind of Coater	Air-to-Air
Substrate material	Aluminum Strip
Maximum substrate width (m)	1000 mm
Substrate thickness	0.3–0.5 mm
Kind of process	Continuous coating
Coating speed	1 m/min
Substrate temperature	200 °C
Dual magnetron sputtering sources	5
DC magnetron sputtering sources	2
Productivity	appr. 0.2 Mio m^2

Table S5. Chemical constituents of the Al strip in the air-to-air produce line.

Chemical constituents (Mass fraction) /%								
Purity (1050)	Impurity content							
Al	Cu	Si	Fe	Zn	Ti	Mn	Mg	V
99.50	<0.05	<0.25	<0.40	<0.05	<0.03	<0.05	<0.05	<0.05

The modularity of the ZDJ–WX–1250 line for the realization of surface cleaning and coating processes of aluminum strip, which mainly consists of three systems to carry out the complete process: (1) wet pre-surface treatment, (2) vacuum equipment comprising an entry lock system, radiation heater for removing the physically adsorbed water from Al strip, a vacuum pre-treatment chamber (glow discharge devices), sputter chambers (10 pcs. expected), chambers for gas separation between sputtering, exit lock chamber, (3) the strip transportation comprising an unwinder unit, a rewinder unit, 2 tension-sensor rollers, 2 cutting device unit, 2 connecting device unit, 2 strip accumulator unit, a dancing roller system for tension control, an edge position control system and several transfer rollers (Fig. 6, Fig. S12). The computer control system realizes the automatic control of the production process without the intervention of the operator, and ensures the consistency and accurate repeatability of the product quality.

A properly designed wet-chemical surface cleaning scheme was first used to remove residual oil stain of the aluminum strip, subsequently was heated up to 200 °C by radiation heater. During heating, physically adsorbed water is removed from the aluminum strip. Then aluminum strip entered into vacuum pre-treatment chamber through entry lock system. The aluminum surface is cleaned by pulse high voltage (2000 V) plasma glow discharge before deposition, which can efficiently remove surface residual impurities and oxide layers, thus to guarantee an excellent adhesion of the coatings in all cases.

The layer deposition takes place in the vertical middle chambers of the production line. Different types of vacuum pumps include mechanical pump, roots pumps, and molecule pumps are used to maintain controlled vacuum conditions in different chambers. High

pumping capacity in the 10^{-3} Pa range is realized in the sputtering chambers by the installation of molecular pumps. All single layers are deposited by magnetron sputtering. The sputtering chambers are equipped with 2 DC-powered magnetrons and 5 MF-powered (20 kHz) dual magnetrons with high purity metallic Al targets (99.99%). Thus, the stable reactive high-rate deposition of highly insulating AlN_xO_y can be achieved. The sputtering atmosphere is composed of argon, oxygen and nitrogen gases. Sputtering from a high purity Al metallic target in Ar, O_2 and N_2 gases promoted the formation of the AlN_xO_y thin films. Consequently, high quality AlN_xO_y thin films were able to be deposited without using costly AlN and Al_2O_3 targets. The first dual magnetron is used for the deposition of the Al layer as infrared reflective and bonding layer. The following double Al–AlN_xO_y nanocermet absorber layers are deposited by 2 dual magnetrons. The Ar/N_2+O_2 ratio was adjusted in a way that resulted in the appropriate Al content of the Al–AlN_xO_y layer. The remaining 3 dual magnetrons serve for the deposition of stoichiometric AlN_xO_y antireflective layer. Some important technical data are compiled in Table S4.

References

[1] M. Kotilainen, K. Mizohata, M. Honkanen, P. Vuoristo, Sol. Energy Mater. Sol. Cells 120, 2014, 462.

[2] M. Koželj, A.Š. Vuk, I. Jerman, B. Orel, *Sol. Energy Mater. Sol. Cells* **2009**, 93, 1733.

[3] M. Köhl, M. Heck, S. Brunold, U. Frei, B. Carlsson, K. Möller, *Sol. Energy Mater. Sol. Cells* **2004**, 84, 275.

[4] S. Brunold, U. Frei, B. Carlsson, K. Moller, M. Kohl, *Sol. Energy* **2000**, 68, 313.

[5] T. C. Diamantino, R. Gonçalves, A. Nunes, S. Páscoa, M. J. Carvalho, *Sol. Energy Mater. Sol. Cells* **2017**, 166, 27.

[6] T.E. Graedel, *J. Electrochem. Soc.* **1989**, 136, 204C.

[7] Z. Dan, I. Muto, N. Hara, *Corros. Sci.* **2012**, 57, 22.